Mineralogy and Petrology (2018) 112 (Suppl 2):S397–S410
https://doi.org/10.1007/s00710-018-0630-7

ORIGINAL PAPER

Kimberlite emplacement and mantle sampling through time at A154N kimberlite volcano, Diavik Diamond Mine: lessons from the deep

Stephen W. Moss[1] · Alan Kobussen[2] · William Powell[2] · Kari Pollock[3]

Received: 30 November 2017 / Accepted: 16 August 2018 / Published online: 15 September 2018

Abstract

The Diavik Diamond Mine in the NWT of Canada has produced in excess of 100 million carats from 3 kimberlite pipes since mining commenced in 2002. Here, we present new findings from deep (>400 m below surface) mining, sampling and drilling work in the A154N kimberlite volcano that require a revision of previous geological and emplacement models and provide a window into how the sub-continental lithospheric mantle (SCLM) below Diavik was sampled by kimberlite magmas through time. Updated internal geological models feature two volcanic packages interpreted to represent two successive cycles of explosive eruption followed by active and passive sedimentation from a presumed crater-rim, both preceded and followed by intrusions of coherent kimberlite. Contact relationships apparent among the geological units allow for a sequential organization of as many as five temporally-discrete emplacement events. Representative populations of mantle minerals extracted from geological units corresponding to four of the emplacement events at A154N are analyzed for major and trace elements, and provide insights into the whether or not kimberlites randomly sample from the mantle. Two independent geothermometers using clinopyroxene and garnet data indicate similar source depths for clinopyroxenes and G9 garnets (130–160 km), and suggest deeper sampling with time for both clinopyroxene and garnets. Harzburgite is limited to 110–160 km, and appears more prevalent in early, low-volume events. Variable ratios of garnet parageneses from the same depth horizons suggest random sampling by passing magmas, but deeper garnet sampling through time suggests early preferential sampling of shallow/depleted SCLM. Evaluations of Ti, Zr, Y and Ga over the range of estimated depths support models of the SCLM underlying the central Slave terrane.

Keywords Sub-continental lithospheric mantle (SCLM) · Kimberlite · Geothermobarometry · Emplacement · Clinopyroxene · Garnet

Introduction

The Diavik Diamond Mine in the NWT of Canada (Fig. 1a, b) has produced in excess of 100 million carats from 4 kimberlite pipes (A154N, A154S, A418, A21) since mining commenced in 2002, and all four pipes are currently being mined for diamonds by Rio Tinto and Dominion Diamond Corporation. The kimberlite pipes and dykes at Diavik were emplaced into Late Archaean plutonic rocks of the central Slave Province (Padgham and Fyson 1992). Geology work to support mining has generated new insights into the nature of the Diavik kimberlite pipes to depths >700 m below surface (Moss et al. 2018), including A154N. A154N is located northeast of A154S and southwest of A841 (Fig. 1b), and is steep-sided, and subcircular to slightly elongate in plan view in a northeast-southwest direction, and widens with depth before tapering into a narrow conduit at nearly 800 m below the present-day surface. The infill of A154N is dominated by a number of massive deposits of pyroclastic kimberlite with intervening deposits of sedimentary kimberlite in an apparent layer-cake stratigraphy (Moss et al. 2008, 2009, 2018). Age-dating of coherent kimberlite samples from A154N indicate emplacement at 56.0 ± 0.7 Ma (Amelin 1996; Barton 1996), coeval with approximately 40% of the dated volcanism in the Lac de Gras area (Sarkar et al. 2015). The average diamond grade from mining of A154N since 2002 is ~2.4 carats per tonne (ct/t).

Editorial handling: C. M. Hetman

✉ Stephen W. Moss
smoss@terramvero.com

[1] Terram Vero Consulting Inc., Vancouver, Canada

[2] Rio Tinto Exploration, Melbourne, Australia

[3] Diavik Diamond Mines Inc., Yellowknife, Canada

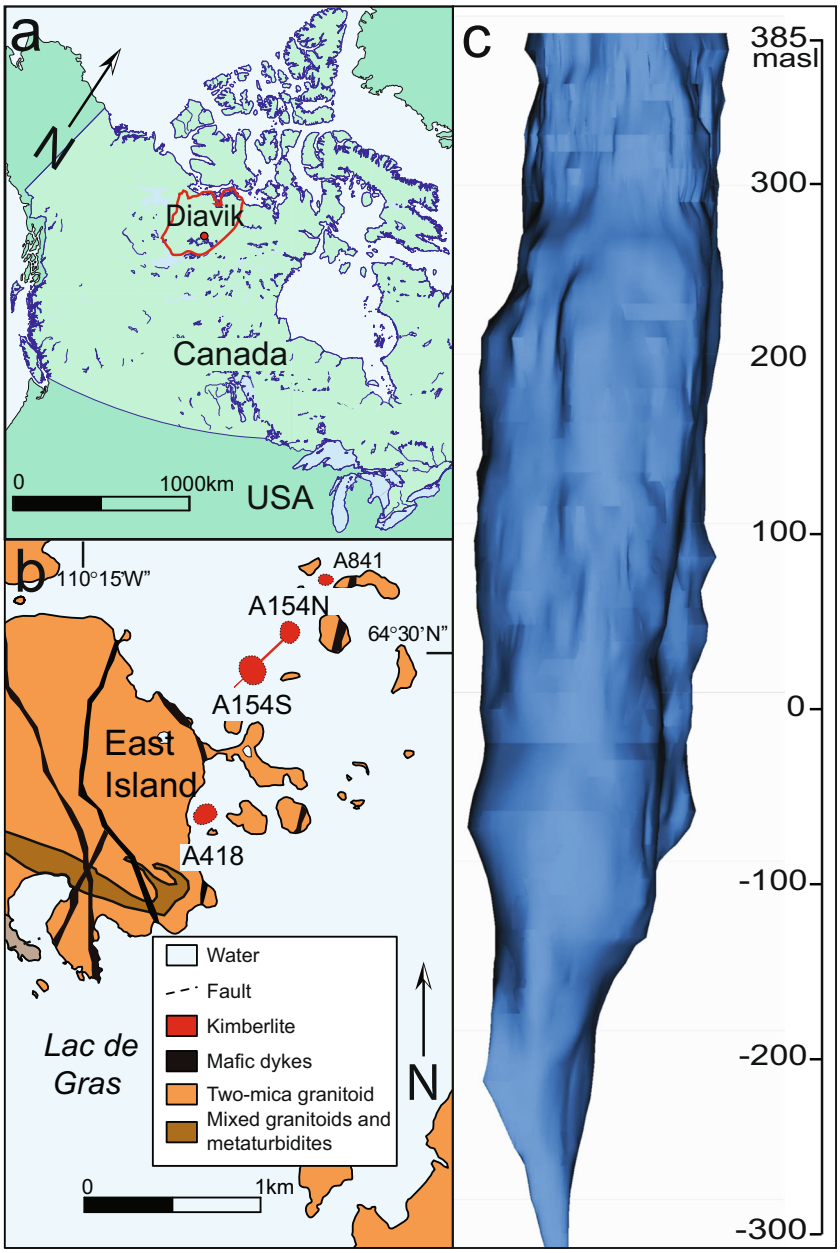

Fig. 1 **a** Location of Diavik within Northwest Territories of Canada, with the Slave craton outlined in red; **b** the kimberlite bodies at Diavik, superimposed on geological mapping of Lac de Gras area from Stubley (1998); **c** 3D pipe shell viewed facing north showing updated morphology of A154N produced in Vulcan™ 3D modelling software

Internal investigations at A154N by Diavik Diamond Mine include logging and sampling for indicator minerals, diamonds, bulk density and petrography from 276 drillcores. Studies on mineral chemistry, bulk density, whole rock chemistry, dilution were also completed. Mapping of underground and open pit exposures, high-resolution (<2 m) survey results and 3D seismic profiles of geological contacts and pipe wall contacts are used to define the pipe geometry. Drillcore logging, underground mapping, and petrography work on A154N completed since 2009 has revealed additional geological domains, and contact relationships apparent among the geological domains allow for a sequential organization of emplacement events. The known relative timing of emplacement of 4 temporally-discrete kimberlite magmas bearing mantle mineral grains into the A154N volcano (Moss et al. 2018) provides an opportunity to investigate how the mantle has been sampled through time by passing kimberlite magmas.

Previous research of the central Slave sub-continental lithospheric mantle (SCLM) has mapped stratigraphy based on large, cluster- or craton-wide datasets (Bostock 1998; Griffin et al. 1999; Griffin et al. 2003; Kopylova et al. 2016; Kopylova and Russell 2000; Yuan and Romanowicz 2010). Sample support for petrological or lithogeochemical studies of the mantle below the Slave Craton commonly comprises heavy mineral grains, mantle xenoliths or diamonds collected from tailings (e.g. Pearson et al. 1999), drill core (e.g. Aulbach et al. 2007), or limited exposures in an open pit of a mine (Creighton et al. 2010; Schmidberger et al. 2005). In the

absence of known sample provenance, these samples are commonly attributed to a kimberlite pipe as a whole (e.g. Griffin et al. 1999; Tappert et al. 2005). Individual kimberlite pipes are shown to commonly comprise deposits resulting from numerous discrete kimberlite magma emplacement events (Scott Smith and Smith 2009). Moreover, distinct mantle samples have been shown to exist among different geology units within a single kimberlite pipe (Galloway et al. 2009), suggesting that poorly-characterized sampling has the potential to mischaracterize the modality or relative proportions of mantle rocks or mineral compositions, and thus any derivative thermobarometry calculations.

Though A154N has been age-dated to 56.0 ± 0.7 Ma (Amelin 1996), there is no geological domain-scale resolution on emplacement ages, and so the full time scale of volcanism is unknown. If the events at A154N occurred within the errors of the available age-dating, which, though untested, is likely, they can be considered geologically coeval. This implies the thermal and barometric conditions of the mantle throughout the life of the A154N volcano were unlikely to have changed. The known internal geology and organized emplacement events at A154N allow for a more detailed approach to studying the SCLM: investigating the sampling of mantle by time-ordered, coeval kimberlite magmas which arrive at effectively a single point at surface.

The mantle cargo within a given kimberlite magma and its resulting deposit are not considered representative of the entire vertical column of mantle lithosphere below, and instead is commonly interpreted to indicate random sampling of the mantle (Downes 1990; Gurney and Switzer 1973; Menzies and Murthy 1980). Representative populations of mantle minerals extracted from the various geological units corresponding to discrete kimberlite magmas at A154N are analyzed for major and trace elements. This careful sampling allows us to test the hypothesis that kimberlite magmas passing through the lithospheric mantle randomly sample available material, and provides insight into the nature of the mantle sampled through time by coeval magmas ascending into a single kimberlite volcano.

Updated A154N geology

Drillcore logging, underground mapping and petrographic study attending mining in A154N since 2009 has revealed two additional geological domains, modified the external shape of A154N (Fig. 1c), and provided additional information about internal contact relationships. This new information is incorporated into an updated 3D internal geological model, and comprises a total of 7 main diamondiferous geological domains, shown schematically in Fig. 2. The updated internal geology improves upon previous interpretations (Moss et al. 2008, 2009), and features two volcanic packages, each comprising massive, mud-poor, poorly-sorted pyroclastic deposits with minimal country rock clasts overlain by mud-rich, moderately- to well-sorted volcaniclastic deposits (i.e. PK1-N/MRVK1-N and PK3-N/MRVK2-N; Moss et al. 2018).

Pipe excavation and deposit emplacements within A154N were preceded by emplacement of coherent kimberlite intermittently within what is now known to have been a pre-existing structure known as "Dueys" striking at 030° (Moss et al. 2018). Importantly, the Dueys structure and the CK1-N it contains were both clearly cross-cut by excavation of the A154N pipe. At the base of the volcano is the newly-identified PK1-N: a massive, crystal and clast-supported pyroclastic kimberlite observed over more than 100 vertical meters at the bottom of the pipe. Though PK1-N is broadly similar with the volumetrically dominant PK3-N domain that occurs higher up in the stratigraphy, it is distinguished from PK3-N because it is spatially-separated by intervening units, has notably less fine ash in the interclast matrix, has noticeably more harzburgite, and lacks alteration. PK1-N is interpreted as a deposit derived from a relatively early (though possibly not the earliest) eruptive event at A154N that fills only 8% of the present-day pipe. PK1-N is capped by previously un-recognized, mud-rich sedimentary deposits which were identified in the recent drilling – MRVK1-N - that cover nearly the entire width of the pipe, but do not contain a significant proportion of volcaniclastic kimberlite autoliths or country rock xenoliths (Moss et al. 2018). MRVK1-N comprises a mixture of chaotic, mud-rich debris avalanche deposits, tractional grain flows, and thin laminar mudstone, with un-disturbed bedding plane orientations determined from vertical drill holes ranging from near horizontal to 35° dip. The only exception to MRVK1-N covering the pipe width is in the NE where vertical, crystallized kimberlite dykes cross-cut the contact between MRVK1-N and PK1-N. The MRVK1-N is also distinct from the pyroclastic deposits at A154N because it contains the highest proportion of indicator mineral grains per kg of any deposit at Diavik and has a low proportion of eclogite. The small volume PK2-N may represent a collapsed block of surface material or a deposit derived from a smaller-scale eruption; contacts are sharp with MRVK1-N with no obvious disconformities. Overlying MRVK1-N and PK2-N is PK3-N. PK3-N is the dominant pipe infill at A154N and is interpreted to have erupted through PK1-N and MRVK1-N along the pipe margin on the NE side of the pipe where crystallized hypabyssal dykes are observed today (Fig. 2). This is a modification of previous interpretations published in Moss et al. (2009), such that PK3-N is no longer considered the earliest pyroclastic eruption event recorded in the deposits of A154N. PK3-N is also capped by mud-rich sedimentary deposits (MRVK2-N) that also cover the entire width of the pipe, which are described in full in previous literature (Moss and Russell 2011; Moss et al. 2008, 2009). The MRVK2-N deposit is itself overlain dis-conformably by a poorly to well-sorted, diffusely-

bedded and graded pyroclastic kimberlite. The graded bed of PK4-N was likely sourced from an adjacent, younger volcano. Both PK4-N and MRVK2-N were likely deposited into a crater lake formed after the PK3-N eruption. Late stage coherent kimberlite cross-cuts the deeper pyroclastic and volcaniclastic deposits (CK-N; Fig. 1). Multiple discrete kimberlite dykes cross-cut all the pipe infill and are typically emplaced along the margins of the pipe (CK-N).

This layer-cake architecture is interpreted to represent two successive cycles of explosive eruption from within A154N followed by active and passive sedimentation from a presumed crater-rim, and the whole package of deposits are both preceded (i.e. Dueys or CK1-N) and followed (i.e. CK2-N) by intrusions of coherent kimberlite. The architecture of A154N bears similarities to that of the nearby Koala pipe at the Ekati diamond mine in Lac de Gras (Crawford et al. 2006; Nowicki et al. 2004). The top of A154N is infilled by an externally-sourced graded deposit of pyroclastic kimberlite (PK4-N) captured by and preserved within a maar crater as described by Moss et al. (2008, 2009).

Contact relationships apparent among the geological domains allow for a sequential organization of emplacement events, and identify four temporally-discrete contributions of kimberlite magma within or surrounding A154N: (1) CK1-N; (2) PK1-N; (3) PK3-N; (4) CK2-N. The mantle indicator minerals entrained as xenocrysts or within xenoliths by the four magmatic events are further investigated below to provide insights into the nature of the mantle sampled through time by coeval, yet temporally-discrete magmas ascending into a single kimberlite volcano.

The geological domains corresponding to the four key emplacement events (CK1-N, PK1-N, PK3-N, and CK2-N) are all notably massive deposits comprising homogeneously-distributed components. Observations from drillcore logging and petrography indicate that A154N geological domains contain a high proportion of kimberlite indicator minerals as both isolated xenocrysts with varying degrees of textural modification and in the context of mantle xenoliths (Table 1). Garnet lherzolite, lherzolite, dunite, wehrlite, eclogite and harzburgite up to 20 cm in diameter are locally observed in the drilling and underground mapping of each domain. No harzburgite xenoliths are observed in CK1-N or CK2-N to date. Megacrysts of Cr-diopside and ilmenite >15 mm are ubiquitous in all studied A154N geological domains (>1 per 4.5 m of drilling), and notably abundant in CK1-N and CK2-N (>1/m). Peridotitic and eclogitic garnet grains rarely exceed 5 mm in size, and isolated megacrysts of peridotitic garnet (>15 mm) are very minor. CK1-N, PK1-N, PK3-N and CK2-N all show a generally high degree of textural and mineralogical preservation among mantle xenocryst minerals (e.g. olivine, clinopyroxene, chromite, ilmenite, peridotitic garnet, eclogitic garnet) in drillcore, an observation further supported by the relatively high concentrate yields apparent from mineral chemistry sampling (Table 2). Local occurrences of poor mineralogical preservation occur, manifested by serpentinization of olivine and/or kelyphite rim development on garnets. The most pronounced kelyphite rim development (up to 25% by area/volume of individual grains) occurs in CK1-N and CK2-N with very fresh olivine and is interpreted to reflect deuteric alteration. Combined with the presence of coalified wood (in MRVK1-N and MRVK2-N), and the observation of very minor amounts of internal veining within A154N, this implies there is low likelihood for significant preservation bias on some species of indicator minerals due to hydrothermal alteration.

Sampling and analytical methods

To support an investigation of how the SCLM was sampled through time at a single kimberlite volcano, a statistically significant and representative subset of indicator mineral grains (ilmenite, chromite, peridotitic garnet, eclogitic garnet, clinopyroxene) were extracted from each geological domain in A154N for mineral chemistry analysis through a proprietary picking and grain selection protocol (Table 2). Approximately 10–12 kg of drill core material was sampled from each of the four geological domains with a known time-organized emplacement sequence in A154N, with samples comprising multiple drill core pieces (pieces <0.5 kg) selected systematically over 30 to 140 m intervals considered to be geologically representative (Fig. 3). Country rock and mantle xenoliths were not avoided during sampling, but no large (>3 cm) mantle xenolith were observed on the outside of the core during sampling. Each sample was homogenized and a ~5 kg aliquot was processed to extract mantle-derived heavy minerals. Samples were crushed using both jaw and rotary crushing methods to optimise the liberation of mineral grains in the 0.3 to 2.36 mm size range. Heavy mineral concentrates were extracted from each sample using tetra-bromoethane (specific gravity ~2.96 g/cm^3). Concentrates were riffle split and then sized into −300, +300–425, +425–710, +700–1000, and + 1000 μm fractions, and the +300–425 μm size fractions were hand sorted under binocular microscopes and all mantle-derived mineral grains (garnet; chromite; ilmenite and Cr-diopside) were extracted to establish the abundance of each mineral type. A statistically significant and representative subset of extracted mantle mineral grains was obtained for mineral chemistry analysis through randomized selection (Table 2), with a total of 1106 garnet grains and 289 clinopyroxene grains analyzed from the four combined domains which are the focus of the present study. Major element compositions were determined using a LEO 1450 scanning electron microscope (SEM) with both energy dispersive (ED) and wave-length dispersive (WD) spectrometers (Oxford Instruments). Trace element compositions collected exclusively for garnets were measured using laser ablation inductively coupled plasma mass spectrometry

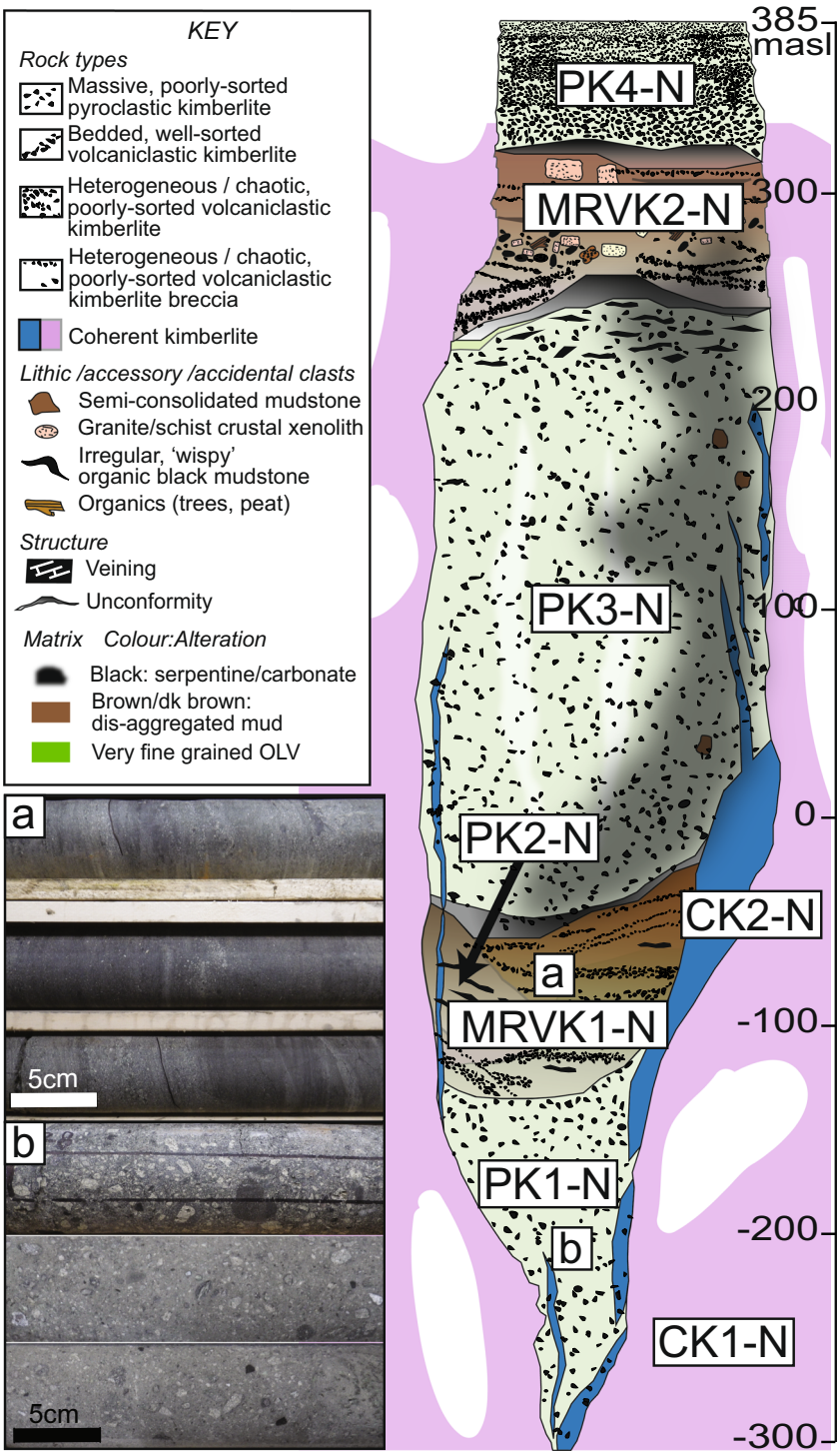

Fig. 2 Schematic cross-section of A154N internal geology facing north-northwest showing key geology units and unique features. The key geology units comprise PK1-N, PK2-N, PK3-N, PK4-N, MRVK1-N, MRVK2-N and CK1-N and CK2-N (see text for descriptions). Schematic legend is shown at upper left. CK1-N (light purple) occurs intermittently within a vertical structure (i.e. Dueys) oriented perpendicular to the northwest-facing view direction

(ICP-MS) over three analytical sessions. Two sessions were conducted using an Agilent 7700 or 7900 ICP-MS coupled to an ASI RESOlution 193 nm excimer laser. The third session was conducted with an Agilent 7900 ICP-MS with an NWR-213 laser fitted with a TV2 cell. The ablation cell was flushed with He as a carrier gas (350 mL/min for the ASI laser, 700 mL/min for the NWR laser), which was mixed with 1.05 L/min of Ar before introduction into the ICP-MS. Laser energy was between 4.6 and 5 Jcm^{-2}, with a 40 (NWR) or 44 (ASI) micron spot and a pulse rate of 5 Hz. GSD-1G was used as the calibration standard, and the internal standard element was ^{43}Ca. BCR2G and NIST610 were included in the runs as secondary standards. Analysis of standards from all three sessions returned results within two standard deviations of the expected value, and no systematic differences are apparent between standards results from the two instruments used in the study.

Table 1 Summary of logged indicator mineral abundances[a] for A154N geology domains

Domain	Number of counts	Red/purple garnet[b] (average # per count)	Orange garnet[b] (average # per count)	Oxide[b] (average # per count)	Chrome diopside[b] (average # per count)
MRVK1-N	155	38.6	2.3	3.1	13.5
MRVK2-N	83	24.0	1.0	0.5	18.0
PK1-N	72	23.6	3.9	1.6	9.3
PK2-N	26	35.9	3.2	4.0	13.8
PK3-N	295	22.0	2.7	1.7	8.2
PK4-N	115	37.0	5.0	0.6	14.0
CK1-N	6	31.0	3.5	6.0	5.2
CK2-N	40	13.0	1.1	1.5	5.3

[a] Kimberlite indicator mineral counts measured from a 2 cm by 20 cm box on the surface of the drill core; values expressed as averages of the number of counts

[b] Visual identification groups used during logging are different to mineral identification recognized by analytical work and are as follows: Red/Purple (i.e. peridotitic) garnet, Orange (i.e. eclogitic) garnet, Oxides (Ilmenite & Chromite), and Chrome diopside

Garnet grains were classified based on their compositions according to Grütter et al. (2004), and chromites were classified according to Fipke et al. (1995) as high-Ti possible phenocrysts, low-Ti possible mantle xenocrysts, or compositionally similar to chromite found in diamond inclusions (DI). Chrome diopside compositions were used to estimate thermobarometric conditions of formation using methods described in Nimis and Taylor (2000). The empirical Ni-in-garnet thermometer as described by Ryan et al. (1996) was utilized to calculate equilibration temperatures for peridotitic garnets. Equilibration pressures for garnets were estimated by applying a best-fit geotherm calculated from clinopyroxene compositions using FITPLOT™ (Mather et al. 2011). Calculated garnet and Cr-diopside pressures were translated to equivalent depths using an assumed density profile comprising 80% lithospheric mantle ($\rho = 3.30$ g/cm^3) and 20% lithospheric crust ($\rho = 2.65$ g/cm^3).

Results

Relative proportions of indicator minerals

A significant number of mantle indicator minerals (ilmenite, orange garnet, red/purple garnet, chromite and Cr-diopside) were recovered from samples from the four domains in this study (Tables 1 and 2) and a subset of the grains were analyzed and probe-verified indicator mineral totals were normalized to total grains per kilogram using the MantleMapper™ protocol (Tables 1 and 2). Summary statistics for indicator minerals from the geological domains in A154N are shown along with sampling grades from large diameter drilling in Tables 1 and 2; statistics for geological domains from the other Diavik pipes and estimates of sampling variance using the same sampling approach are shown by Moss et al. (2018). Analysis of the calculated abundances from all domains in A154N suggests that domains can be grouped into four different classes based on the relative proportion of indicator mineral grains (Fig. 3); a fifth class is represented by the CK1-N pre-cursor coherent kimberlite intrusion into existing structure. Group (a) is charaterized by a high proportion of eclogite, and very low to low proportions of ilmenite and chromite, and comprises three different deposits of pyroclastic kimberlite: PK2-N, PK3-N and PK4-N. Group (b) is characterized by a high proportion of clinopyroxene grains and relatively low eclogite component, and comprises mud-rich volcaniclastic kimberlite deposits: MRVK1-N and MRVK2-N. Group (c) comprises the late stage intrusions of coherent kimberlite which cross-cut the deeper deposits in A154N (CK2-N), and is distinguished by relatively high proportions of clinopyroxene, and low proportion of megacrystic garnet. Group (d) is characterized by a high eclogite component and the highest proportion of chromite in A154N, and comprises the earliest and deepest pyroclastic deposit, PK1-N. Group (e) comprises the pre-cursor coherent kimberlite intrusion into existing structure at the A154N locale, and is characterized by a distinctly high proportion of ilmenite and megacrystic garnet. Domain-specific results were weighted by relative domain tonnages to come up with a total estimate for A154N of the absolute abundances and relative proportions of different mantle indicator minerals (Moss et al. 2018; Fig. 3). The same exercise was completed for the other project pipes at Diavik (A154S, A418, A21), and are compared to A154N in Fig. 4 and summarized by Moss et al. (2018). There are some broad similarities among some of the project pipes at Diavik in mantle componentry, but A154N has a noticeably higher proportion of eclogitic garnet, with three times (3×) that observed in A154S and A418, and one and a half (1.5×) that observed in A21. The primary pyroclastic deposits are the main sources of the high eclogite component, while the sedimentary deposits have a lower eclogite component.

Table 2 Summary of probe-corrected indicator mineral abundances and sample diamond grades for A154N geology domains

Domain	Sample grade (ct/t)	Concentration yield (%)[a]	Logged mantle xenoliths / megacrysts	Pgar		MegGar		Egar		Ilm		Chr		Cd		Total	
				Number of analyes[b]	Abundance (per kg)[c]	Number of analyes[b]	Abundance (per kg)[c]	Number of analyses[b]	Abundance (per kg)[c]	Number of analyes[b]	Abundance (per kg)[c]	Number of analyses[b]	Abundance (per kg)[c]	Number of analyes[b]	Abundance (per kg)[c]	Number of analyes[b]	Abundance (per kg)[c]
MRVK1-N	2.75	7	gt lherz; lherz; wehrlite; dunite; eclogite; Cd/Ilm/MegGar	114	24,783	24	2,028	71	2,028	81	8,261	18	225	52	15,546	360	52,871
MRVK2-N	2.64	2	gt lherz; lherz; wehrlite; dunite; eclogite; Cd/Ilm/MegGar	219	9,443	33	696	159	1,024	134	673	71	118	106	5,927	722	17,881
PK1-N	2.18	17	gt lherz; lherz; harz; wehrlite; dunite; eclogite; Cd/Ilm/MegGar	119	10,768	9	655	73	3,747	62	738	37	994	62	1,547	362	18,449
PK2-N	n/a	18	gt lherz; lherz; dunite; eclogite; Cd/Ilm/MegGar	118	12,179	16	647	70	3,092	66	1,230	40	94	54	4,958	364	22,200
PK3-N	2.38	33	gt lherz; lherz; wehrlite; dunite; harz; eclogite; Cd/Ilm/MegGar	300	13,196	46	4,556	207	1,520	215	423	140	71	151	6,909	1,059	26,675
PK4-N	4.74	13	gt lherz; lherz; wehrlite; dunite; harz; eclogite; Cd/Ilm/MegGar	122	8,600	11	656	53	1,895	89	155	42	75	40	4,665	357	16,046
CK1-N	n/a	27	gt lherz; lherz; wehrlite; dunite; eclogite; Cd/Ilm/MegGar	105	16,218	27	3,307	41	3,245	91	7,243	51	157	33	4,881	348	35,051
CK2-N	n/a	32	gt lherz; lherz; wehrlite; dunite; eclogite; Cd/Ilm/MegGar	110	2,585	13	130	56	426	73	414	14	17	43	2,835	309	6,407

Abbreviations: Pgar = peridotitic garnet; Egar = eclogitic garnet; MegGar = megacrystic garnet; Ilm = kimberlitic ilmenite; Chr = chromite; Cd = chrome diopside; gt lherz = garnet lherzolite; lherz = lherzolite; Cd/Ilm/MegaGar = chrome diopside/ilmenite/garnet megacrysts; n/a = not available

[a] Percentage of material (all sizes / types) recovered from the initial sample mass by heavy mineral separation using tetra-bromoethane (mass density ~2.96 g/cm^3)

[b] Number of microprobe analyses

[c] Probe-corrected mantle indicator mineral abundances of +300-425 μm grains per kg by geology domain. Visually-identified mineral grain abundances from hand sorting are adjusted by applying ratios of observed:analyzed shown in mineral chemistry results

Variability within A154N matches or exceeds that apparent among the project pipes at Diavik (Fig. 4).

Clinopyroxene thermobarometry

The Nimis and Taylor (2000) single-grain clinopyroxene thermobarometer was used to estimate temperature and pressure of compositionally-filtered clinopyroxene grains. To establish the most reliable geotherm, clinopyroxene grains were further filtered based on updated criteria found in Ziberna et al. (2016), and along with a best-fit geotherm calculated using the FITPLOT method of Mather et al. (2011). Temperature and pressure estimates for all clinopyroxenes from Diavik passing Nimis and Taylor (2000) compositional filters and the grains passing the more restrictive criteria of Ziberna et al. (2016) are shown in Fig. 5, along with calculated geotherms and associated error envelopes. The more restrictive filters proposed by Ziberna et al. (2016) yield a regression showing a slightly warmer geotherm with smaller uncertainties on the fit. Pressures were converted to depths by using an an assumed density profile comprising 80% lithospheric mantle ($\rho = 3.30$ g/cm^3) and 20% lithospheric crust ($\rho = 2.65$ g/cm^3). Calculated depths were weighted according to the relative tonnages of each geological domain to generate depth estimates of the total clinopyroxene population from A154N (Fig. 6). Calculated depths from cpx grains indicate that garnet lherzolite from the SCLM sampled by the kimberlite magmas feeding A154N ranged from depths of 100 km to 200 km depth. More than 75% of the grains from A154N are sourced from the 140–160 km depth range, and a relatively even distribution of the remaining grains are sourced from >160 km. More than 75% of the grains among all domains are sourced from the 110–160 km depth range, and a relatively even distribution of the remaining grains are sourced from >160 km.

The eruptive time sequence established above from crosscutting relationships at A154N shows an apparent change in sampling depth with time. Calculated depths appear to suggest there is a progressively deeper sampling of mantle clinopyroxene, and by inference mantle lherzolite, through time. Early or older events sampled shallower lherzolite, while later or younger events sampled more deeply.

Garnet thermobarometry

The empirical Ni-in-garnet thermometer from Ryan et al. (1996) was utilized to calculate equilibration temperatures ($T_{\mathrm{Ni\ in\ gt}}$) for peridotitic garnets. Garnet pressures were estimated by applying the best-fit geotherm determined using clinopyroxenes in FITPLOT to $T_{\mathrm{Ni\ in\ gt}}$ for peridotitic garnet grains. Pressures were converted to depths using the same assumed density profile as for the clinopyroxenes, and garnet and clinopyroxene depths are shown in Fig. 7. More than 80% of the grains among all four events are sourced from 120 to 170 km, and the highest frequency of garnets were sampled from 130 to 150 km. The depths for G9 or lherzolitic garnets correlate well with those of the clinopyroxenes, and garnets as a whole show a similar increase in sampling depth with time as demonstrated by the clinopyroxenes. Harzburgitic garnets shows a restricted range of sampling, with no harzburgitic garnet sourced from >160 km depth. One event (PK1-N) shows a distinctively higher relative proportion of harzburgite than the others, and shows lherzolitic, harzburgitic and high-Ti peridotitic garnets are present in similar abundances from 130 to 160 km. The same depth horizons show different ratios of G9/G10/G11 garnets among the four events (e.g. 150–160 km).

Trace element compositions

The Zr, TiO_2, Y and Ga compositions of peridotitic garnets are evaluated over the range of estimated depths to test models of the SCLM underlying the central Slave

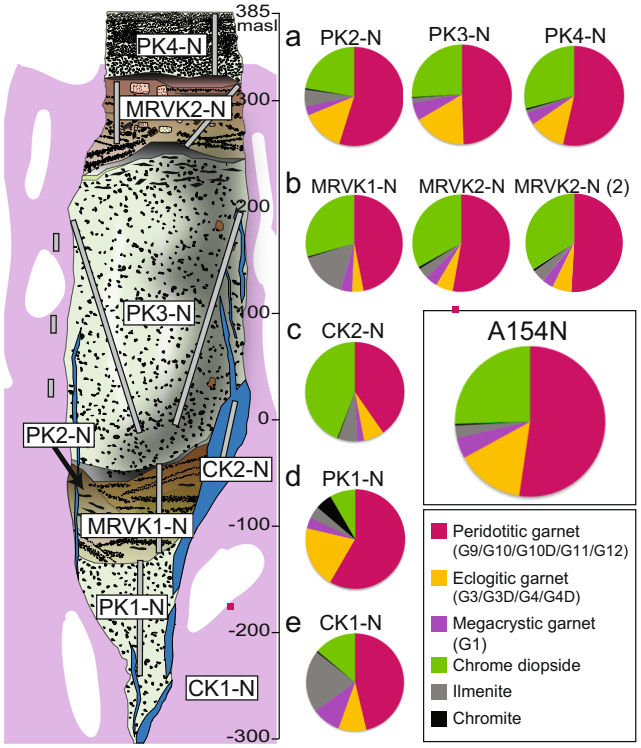

Fig. 3 Relative abundances of +300-425 μm indicator mineral grains (peridotitic garnet, eclogitic garnet, megacrystic garnet, Cr-diopside, ilmenite, chromite) from geology domains in A154N. Garnets are classified after Grütter et al. (2004). Five distinct mantle mineral populations are apparent among the 8 different geological domains, and are labelled (**a**) to (**e**). Absolute abundances of +300-425 μm grains per kg are weighted by domain tonnage and combined to generate an estimate of the relative abundances for all of A154N, shown in the inset at right. Sample locations within geological domains are indicated by grey bars in the schematic at left

terrane (Fig. 8). There are no systematic differences among the four events, but results show an increase in Y, Zr and TiO_2 corresponding to depths of approximately 150–160 km. This is broadly consistent with some mantle stratigraphy models in the literature for the central Slave which suggest the presence of a two-layer lithospheric mantle comprising a depleted to ultra-depleted upper layer above 150 km depth, and a less-depleted lherzolitic layer below (Griffin et al. 1999; Menzies et al. 2004).

Discussion

Variability in indicator mineral proportions

Apparent differences in relative proportions could reflect variance related to sampling (e.g. unrecognized local changes within a geology domain, the presence/absence of megacrysts), analytical variance, preservation bias, or a bias introduced through the processing methodology (e.g. abundances and analyses deriving from a restricted size fraction). Outsized (>20 mm) clinopyroxene megacrysts are capable of influencing estimates of the relative proportions of clinpyroxene and other indicator minerals. However, clinopyroxene megacrysts are present in all the A154N deposits, and, combined with the high number of clinopyroxene grains in indicator mineral counts from drill core and the absence of statistically-dominant calculated temperatures (Fig. 7), suggest the influence of outsized (megacrystic) grains to most likely be minor. The sampling and analytical variance indicated by domains with multiple samples at Diavik analyzed in different batches are less significant than the differences within a single pipe (Moss et al. 2018). The potential bias introduced by reviewing only the +300-425 μm size fraction from a crushed and homogenized sample is considered more likely to minimize variability than to enhance it. As preservation bias is considered unlikely in such fresh kimberlite rocks, the apparent differences among domains in a single pipe are thus interpreted to represent differences in the mantle sampled by kimberlite magmas that produced the deposits.

The relative proportions of kimberlite indicator minerals among the various geological units in A154N indicate that variability in proportions of kimberlite indicator minerals within a pipe can match or exceed that apparent among the kimberlite pipes in a cluster. This highlights the importance of resolving the geological context of mantle mineral samples: sampling from non-representative or only limited geological domains for indicator mineral populations can mask hidden populations of interest within a pipe. Changes in the scale and/or thoroughness of sampling could lead to very different pictures of mantle stratigraphy.

Random and non-random mantle sampling

Two independent geothermobarometers using clinopyroxene and garnet data point to similar source depths for lherzolitic

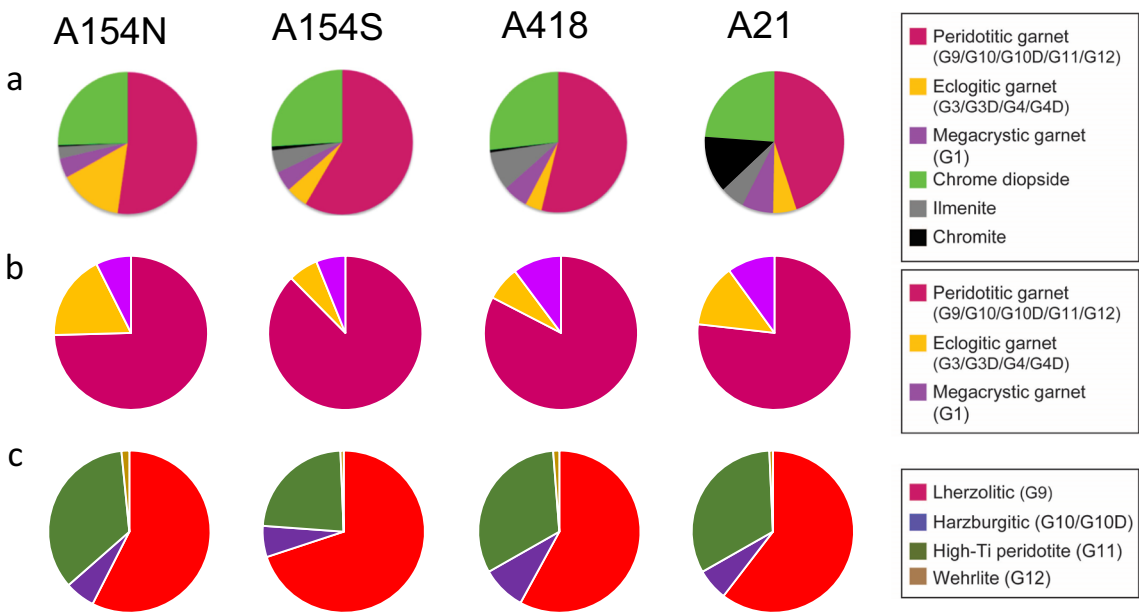

Fig. 4 Relative abundances of indicator mineral grains in the +300-425 μm size fraction. Absolute abundances of +300-425 μm grains per kg are weighted by domain tonnage and combined to generate an estimate of the relative abundances for each of the Diavik project pipes for: **a** all indicator mineral types (peridotitic garnet, eclogitic garnet, megacrystic garnet, Cr-diopside, ilmenite, chromite); **b** major garnet types (i.e. peridotitic garnet, eclogitic garnet, megacrystic garnet), and **c** peridotitic garnet parageneses (i.e. lherzolitic, harzburgitic, high-Ti peridotite, and wehrlite). Garnets are classified after Grütter et al. (2004)

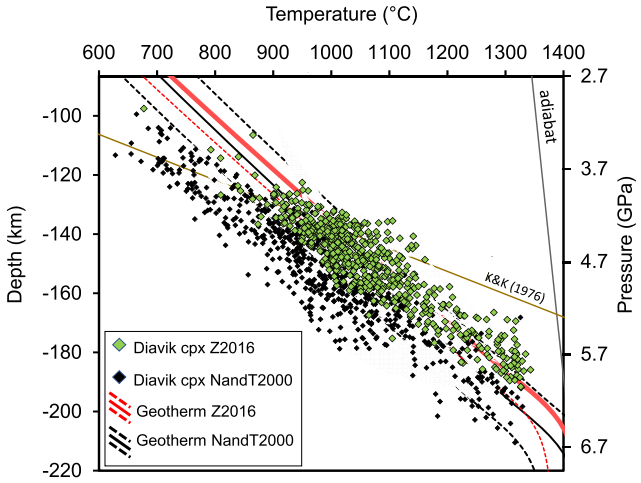

Fig. 5 Clinopyroxene thermobarometry and mantle geotherm for the central Slave craton sampled by the four project kimberlites at Diavik (A154N, A154S, A418 and A21). All clinopyroxene results were compositionally-filtered to reduce potential errors according to methods described in Nimis and Taylor (2000; NandT2000) and Ziberna et al. (2016; Z2016), generating different datasets. Separate FITPLOT regressions were generated for each dataset, with the Z2016 dataset resulting in smaller uncertainties to the fit, and therefore a more reliable geotherm for Diavik. Mantle adiabat is shown with grey line; graphite-diamond transitions of Kennedy and Kennedy (1976) are shown for reference

components, which is dominantly from 130 to 160 km, but apparently sample more deeply through time. Harzburgite is limited to 110–160 km, and seems to be more prevalent in early, low-volume events. There is a clear increase in a number of trace elements at depths greater than 160 km. Variable garnet type ratios are present from the same depth horizons, suggesting that passing

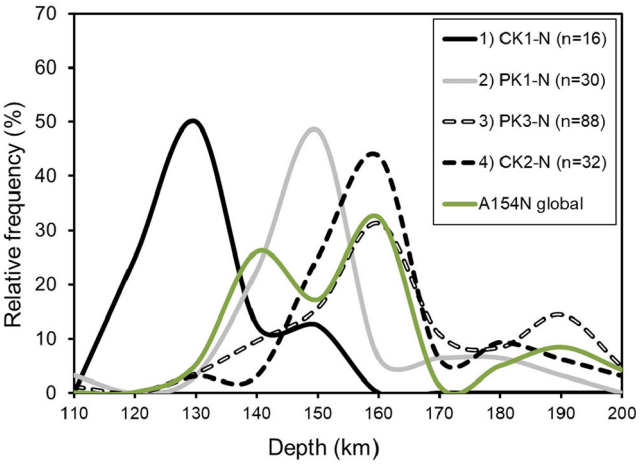

Fig. 6 Relative frequency histogram of calculated depths of formation for clinopyroxene from four magmatic events at Diavik. The number of analysed grains for each event are indicated in parentheses in the legend. Clinopyroxene sample depths are weighted by relative geological domain tonnage for all A154N domains (including MRVK1-N, MRVK2-N, PK2-N, PK4-N) to generate a global relative frequency histogram for A154N shown in green

coeval magmas emplaced at A154N are in fact randomly sampling from a heterogeneous mantle at any given depth horizon. However, the successively deeper sampling indicated by garnet lherzolite thermobarometry suggest that sampling depth is not random, but instead exhibits a preferential sampling of shallow (110 to 140 km) and/or more depleted mantle lithosphere by earlier lower-volume magmas, followed by successively higher proportions of deeper, more geochemically fertile mantle sampled by larger volumes of kimberlite magma at A154N. The depth constraints of harzburgitic garnets and the observations of a shift to higher trace element concentrations at ~160 km both broadly support the prevailing two-layer model for the central Slave sub-continental lithosphere comprising a more depleted upper layer and a less depleted lower layer (Griffin et al. 1999; Kopylova and Russell 2000; Menzies et al. 2004).

Model for mantle sampling by kimberlite magmas through time

The extent to which the findings from A154N are replicated at other poly-magmatic kimberlite volcanos remains to be seen, but the well-constrained facies analysis at A154N combined with mineral chemistry and thermobarometry results described allow for development of a working hypothesis for the manner in which kimberlite magmas sample from the underlying SCLM. To this end, an interpreted model for mantle sampling by kimberlite magmas based on the findings at A154N is shown schematically in Fig. 9.

Variable garnet type ratios from a given depth horizon point to lateral compositional heterogeneity, adding complexity to a simple two-layer model (Fig. 9). Such compositional heterogeneity may reflect localized episodic metasomatic enrichment and/or compositional depletion throughout the history of the SCLM below Diavik (Aulbach et al. 2013; Creighton et al. 2007). The scale of lateral compositional heterogeneity is unknown (m's or km's?), but boundaries between adjacent zones of compositionally-distinct material may be locales of structural weakness exploited by ascending kimberlite fluids or magmas. Early fluid or magmatic events transiting through the SCLM create pathways which are exploited by subsequent events, culminating in shared pathways in the near surface crustal environment and expression into the same kimberlite volcano. The time lag between events must be short enough that pathways through the SCLM retain memory of stress in conduit walls and/or in the rock fabric. Magmas ascending in the lithospheric mantle strain adjacent wall rocks by crack tip propagation (Brett et al. 2015; Russell et al. 2012), as well as by fluid pressure from intruding or

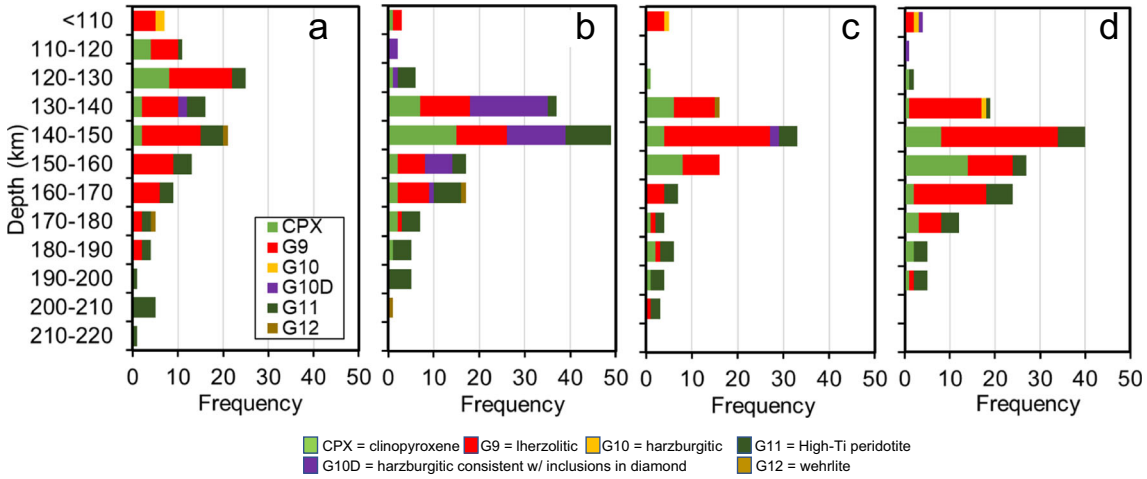

Fig. 7 Histograms of calculated depths of formation for clinopyroxene and peridotitic garnets from four magmatic events at Diavik, organized in time sequence in panels (**a**) to (**d**) (left to right). Garnet temperatures were determined using the Ni in garnet thermometer of Ryan et al. ($T_{Ni\ in\ gt}$; 1996). $T_{Ni\ in\ gt}$ were translated to equivalent pressures and depths by using a FITPLOT™ geotherm (Mather et al. 2011) generated from Diavik clinopyroxene tempterature and pressure values obtained using techniques described in Ziberna et al. (2016). Clinopyroxene data are also plotted, and show two independent geothermobarometers (Nimis and Taylor 2000; Ryan et al. 1996) point to similar source depths for lherzolitic components [i.e. clinopyroxene and lherzolitic (G9) garnets]

passing metasomatic fluids or kimberlite magmas (Drury et al. 1991). This strain is absorbed by developing shear planes and/or reduced grain size via recrystallization (Drury and Van Roermund 1989) in the ductile mantle, and in so doing generates ideal pathways of structural weakness for subsequent fluids or magmas.

We suggest that the sampling of garnet-bearing mantle peridotite from increasing depths through time is a reflection of assimilation of conduit walls from ever-deepening zones of weakness in the SCLM induced by intruding and/or transiting metasomatic fluids, kimberlitic fluids and/or kimberlitic magmas. This interpretation is further supported by observations of olivine in kimberlites, indicating a modal and numerical dominance by grains <2 mm in size, with crystal size distributions that obey power laws consistent with porphyroclastic peridotite (Armienti and Tarquini 2002; Moss et al. 2010), and in at least some cases are dominantly xenocrystic in origin (Arndt et al. 2010; Brett et al. 2009, 2015). These olivine appear distinct from the coarse and equigranular olivine observed in many peridotite xenoliths found in kimberlites (Harte 1977; Kopylova et al. 1999; Winterburn et

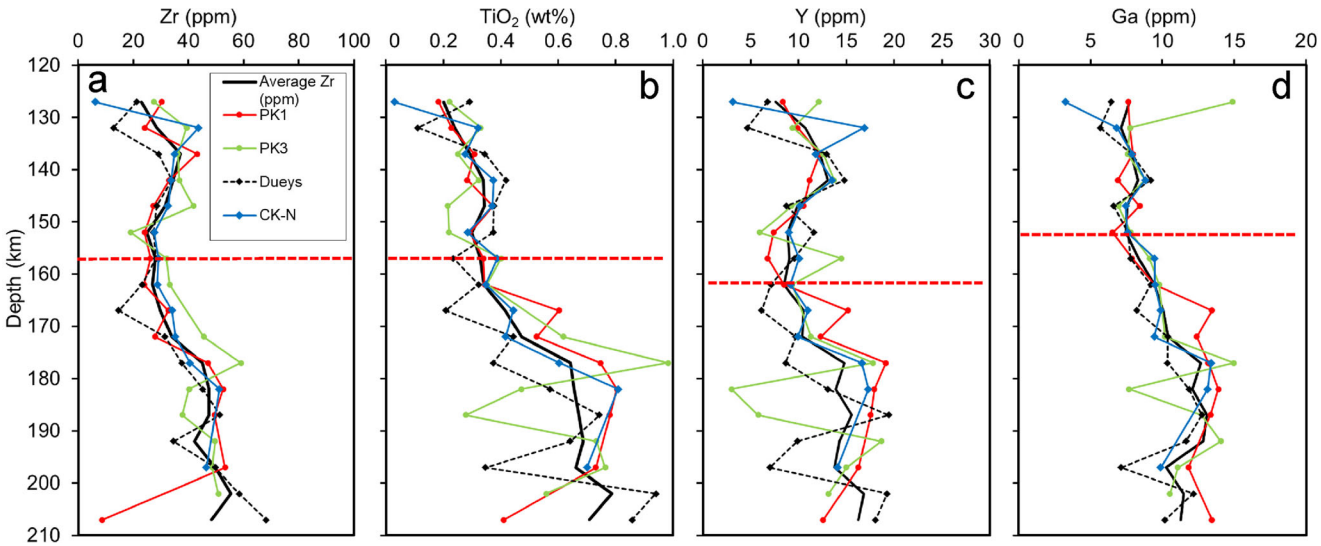

Fig. 8 Trace element (Zr, TiO_2, Y, and Ga) compositions of peridotitic garnets vs. calculated depth (km) for four magmatic events at Diavik. Average values for all combined geology domains by 5 km steps are shown with black lines. Red-dashed line indicates depth of clear increase in abundance of the respective trace elements

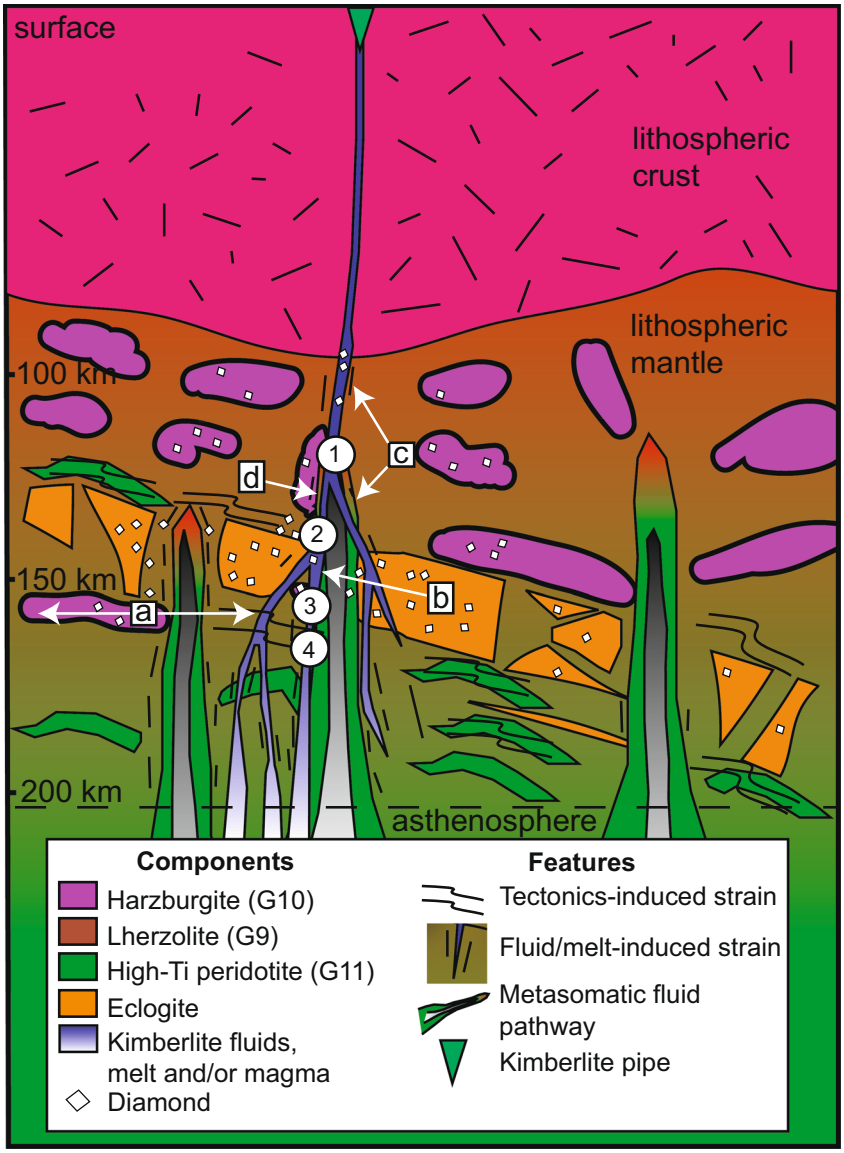

Fig. 9 Schematic illustration showing interpreted model for mantle sampling by kimberlite magmas based on the findings at A154N, with the following features: a) variable garnet type ratios from a given depth horizon point to lateral compositional heterogeneity, reflecting the input of localized, episodic metasomatic enrichment and/or compositional depletion throughout the history of the SCLM; b) boundaries between adjacent zones of compositionally distinct material, generated by either tectonics (i.e. subducted oceanic slab metamorphosed into eclogite) or fluid injection, may be locales of strain and/or structural weakness exploited by subsequent ascending fluids or magmas; c) early fluid or magmatic events transiting through the SCLM create pathways which are exploited by subsequent events, culminating in shared pathways in the near surface crustal environment and expression into the same kimberlite volcano; d) short time lags between events allows old pathways through the SCLM to retain stress memory in conduit walls and/or in the rock fabric by developing shear planes and/or reduced grain size via recrystallization, which in turn facilitate passage and entrainment of weakened mantle by subsequent kimberlite magmas transiting through the area. The sampling of mantle from increasing depths through time (letters a to d) is interpreted to be a reflection of ever-deepening zones of weakness in the SCLM induced by transiting kimberlitic fluids and/or magmas

al. 1990). This difference may in part be explained if olivine recrystallized into very small (<1 mm) subhedral grains, tablets or euhedral grains (Boullier and Nicolas 1975), and/or highly strained olivine from porphyroclastic peridotite are preferentially dis-aggregated and entrained relative to mantle peridotites with hypidiomorphic granular or well-equilibrated granoblastic rock fabrics.

Acknowledgements Thanks to the organisers of the 11th International Kimberlite Conference for the opportunity to present these findings, to the Diavik Diamond Mine geology team for ongoing collaboration, sample collection, and helpful discussions on interpretations. Some excellent laser work was completed by the Rio Tinto Exploration team in Bundoora, Australia and the Center for Ore Deposits and Earth Sciences (CODES) in Hobart, Australia. Thanks to Mineral Services Canada and the University of Stellenbosch for major element microprobe

work and support. Thanks to Herman Grütter, Graham Pearson, Paolo Nimis, Maya Kopylova, Tom Nowicki, Kelly Russell, Curtis Brett, Matthew Field, Pat Hayman, and Lucy Porritt for invaluable comment, critique and discussions. Constructive comments by an anonymous reviewer and guest editor Casey M. Hetman are gratefully acknowledged.

References

Amelin Y (1996) Report on Rb-Sr and U-Pb study of kimberlite samples VR44444A through VR44465A. Confidential report for Kennecott Canada Inc., 6 pp

Armienti P, Tarquini S (2002) Power law olivine crystal size distributions in lithospheric mantle xenoliths. Lithos 65:273–285

Arndt NT, Guitreau M, Boullier AM, Le Roex A, Tommasi A, Cordier P, Sobolev A (2010) Olivine, and the origin of Kimberlite. J Petrol 51: 573–602

Aulbach S, Pearson NJ, O'reilly SY, Doyle BJ (2007) Origins of xenolithic eclogites and pyroxenites from the Central Slave Craton, Canada. J Petrol 48:1843–1873

Aulbach S, Griffin WL, Pearson NJ, O'Reilly SY (2013) Nature and timing of metasomatism in the stratified mantle lithosphere beneath the central Slave craton (Canada). Chem Geol 352:153–169

Barton ES (1996) Rb-Sr Mica age results from the Diavik kimberlite field. Confidential report for Kennecott Canada Inc. 5 pp

Bostock M (1998) Mantle stratigraphy and evolution of the Slave province. J Geophys Res–Sol Ea 103:21183–21200

Boullier AM, Nicolas A (1975) Classification of textures and fabrics of peridotite xenoliths from South African kimberlites. Phys Chem Earth 9:467–468 IN7, 469–475

Brett RC, Russell JK, Moss S (2009) Origin of olivine in kimberlite: phenocryst or impostor? Lithos 112:201–212

Brett RC, Russell JK, Andrews GDM, Jones TJ (2015) The ascent of kimberlite: insights from olivine. Earth Planet Sc Lett 424:119–131

Crawford B, Porrit L, Nowicki TE, Carlson J (2006) Key geological characteristics of the Koala kimberlite, Ekati Diamond Mine, Canada. In: Kimberlite Emplacement Workshop, 8th International Kimberlite Conference. Saskatoon, Saskatchewan, September 7–14, 2006

Creighton S, Stachel T, McLean H, Muehlenbachs K, Simonetti A, Eichenberg D, Luth R (2007) Diamondiferous peridotitic microxenoliths from the Diavik Diamond Mine, NT. Contrib Mineral Petrol 155:541–554

Creighton S, Stachel T, Eichenberg D, Luth RW (2010) Oxidation state of the lithospheric mantle beneath Diavik diamond mine, central Slave craton, NWT, Canada. Contrib Mineral Petrol 159:645–657

Downes H (1990) Shear zones in the upper mantle—relation between geochemical enrichment and deformation in mantle peridotites. Geology 18:374–377

Drury M, Van Roermund HV (1989) Fluid assisted recrystallization in upper mantle peridotite xenoliths from kimberlites. J Petrol 30:133–152

Drury MR, Vissers RL, Van der Wal D, Strating EHH (1991) Shear localisation in upper mantle peridotites. Pure Appl Geophys 137: 439–460

Fipke CE, Gurney J, Moore R (1995) Diamond exploration techniques emphasising indicator mineral geochemistry and Canadian example. Bull Geol Surv Can 423

Galloway M, Nowicki T, van Coller B, Mukodzani B, Siemens K, Hetman C, Webb K, Gurney J (2009) Constraining kimberlite geology through integration of geophysical, geological and geochemical methods: a case study of the Mothae kimberlite, northern Lesotho. Lithos 112(S1):130–141

Griffin W, Doyle BJ, Ryan CG, Pearson NJ, O'Reilly SY, Davies R, Kivi K, Van Achterbergh E, Natapov LM (1999) Layered mantle lithosphere in the Lac de Gras area, Slave craton: composition, structure and origin. J Petrol 40:705–727

Griffin W, O'Reilly SY, Abe N, Aulbach S, Davies RM, Pearson NJ, Doyle BJ, Kivi K (2003) The origin and evolution of Archean lithospheric mantle. Precambrian Res 127:19–41

Grütter HS, Gurney JJ, Menzies AH, Winter F (2004) An updated classification scheme for mantle-derived garnet, for use by diamond explorers. Lithos 77:841–857

Gurney J, Switzer G (1973) The discovery of garnets closely related to diamonds in the Finsch pipe, South Africa. Contrib Mineral Petrol 39:103–116

Harte B (1977) Rock nomenclature with particular relation to deformation and recrystallisation textures in olivine-bearing xenoliths. J Geol 85: 279–288

Kennedy CS, Kennedy GC (1976) The equilibrium boundary between graphite and diamond. J Geophys Res 81:2467–2470

Kopylova MG, Russell JK (2000) Chemical stratification of cratonic lithosphere: constraints from the Northern Slave craton, Canada. Earth Planet Sc Lett 181:71–87

Kopylova M, Russell J, Cookenboo H (1999) Petrology of peridotite and pyroxenite xenoliths from the Jericho kimberlite: implications for the thermal state of the mantle beneath the Slave craton, northern Canada. J Petrol 40:79–104

Kopylova MG, Beausoleil Y, Goncharov A, Burgess J, Strand P (2016) Spatial distribution of eclogite in the Slave cratonic mantle: the role of subduction. Tectonophysics 672:87–103

Mather KA, Pearson DG, McKenzie D, Kjarsgaard BA, Priestley K (2011) Constraints on the depth and thermal history of cratonic lithosphere from peridotite xenoliths, xenocrysts and seismology. Lithos 125:729–742

Menzies M, Murthy VR (1980) Enriched mantle: Nd and Sr isotopes in diopsides from kimberlite nodules. Nature 283:634–636

Menzies A, Westerlund K, Grütter H, Gurney J, Carlson J, Fung A, Nowicki T (2004) Peridotitic mantle xenoliths from kimberlites on the Ekati Diamond Mine property, N.W.T., Canada: major element compositions and implications for the lithosphere beneath the central Slave craton. Lithos 77:395–412

Moss S, Russell J (2011) Fragmentation in kimberlite: products and intensity of explosive eruption. Bull Volcanol 73:983–1003

Moss S, Russell JK, Andrews GDM (2008) Progressive infilling of a kimberlite pipe at Diavik, Northwest Territories, Canada: insights from volcanic facies architecture, textures, and granulometry. J Volcanol Geotherm Res 174:103–116

Moss S, Russell JK, Brett RC, Andrews GDM (2009) Spatial and temporal evolution of kimberlite magma at A154N, Diavik, Northwest Territories, Canada. Lithos 112(S1):541–552

Moss S, Russell JK, Scott Smith BH, Brett RC (2010) Olivine crystal size distributions in kimberlite. Am Mineral 95:527–536

Moss S, Porritt L, Pollock K, Fomradas G, Stubley M, Eichenberg D, Cutts J (2018) Geology, mineral chemistry and structure of the kimberlites at Diavik Diamond Mine: indicators of cluster-scale cross-fertilization, mantle provenance and pipe morphology. Soc Eco Geo Spc Pub 20:287–318

Nimis P, Taylor WR (2000) Single clinopyroxene thermobarometry for garnet peridotites. Part I. Calibration and testing of a Cr-in-Cpx barometer and an enstatite-in-Cpx thermometer. Contrib Mineral Petrol 139:541–554

Nowicki T, Crawford B, Dyck D, Carlson J, McElroy R, Oshust P, Helmstaedt H (2004) The geology of kimberlite pipes of the Ekati property, Northwest Territories, Canada. Lithos 76:1–27

Padgham W, Fyson W (1992) The slave province: a distinct Archean craton. Can J Earth Sci 29:2072–2086

Pearson NJ, Griffin WI, Doyle BJ, O'Reilly SY, Van Achtenburg E, Kivi K (1999) Xenoliths from kimberlite pipes of the Lac de Gras area, Slave Craton, Canada. In: Gurney JJ, Richardson SR (eds) Proceedings of

the 7th International Kimberlite Conference, the PH Nixon Volume, vol 2. Red Roof Design, Cape Town, pp 644–658

Russell JK, Porritt LA, Lavallee Y, Dingwell DB (2012) Kimberlite ascent by assimilation-fuelled buoyancy. Nature 481:352–356 http://www.nature.com/nature/journal/v481/n7381/abs/nature10740.html#supplementary-information

Ryan CG, Griffin WL, Pearson NJ (1996) Garnet geotherms: pressure–temperature data from Cr-pyrope garnet xenocrysts in volcanic rocks. J Geophys Res–Sol Ea 101:5611–5625

Sarkar C, Heaman LM, Pearson D (2015) Duration and periodicity of kimberlite volcanic activity in the Lac de Gras kimberlite field, Canada and some recommendations for kimberlite geochronology. Lithos 218:155–166

Schmidberger S, Heaman L, Simonetti A, Whiteford S (2005) In-situ Pb and Sr and Lu-Hf isotope systematics of mantle eclogites from the Diavik diamond mine, NWT, Canada. Geochim Cosmochim Ac 69(10S):A287

Scott Smith BH, Smith SCS (2009) The economic implications of kimberlite emplacement. Lithos 112:10–22

Stubley MP (1998) Bedrock geology of the East Island area, Lac de Gras. Unpublished internal report prepared for Diavik Diamond Mines Inc., 45 pp

Tappert R, Stachel T, Harris JW, Shimizu N (2005) Mineral inclusions in diamonds from the Panda kimberlite, Slave Province, Canada. Eur J Mineral 17:423–440

Winterburn PA, Harte B, Gurney JJ (1990) Peridotite xenoliths from the Jagersfontein kimberlite pipe: I. Primary and primary-metasomatic mineralogy. Geochim Cosmochim Ac 54:329–341

Yuan H, Romanowicz B (2010) Lithospheric layering in the North American craton. Nature 466:1063–1068

Ziberna L, Nimis P, Kuzmin D, Malkovets VG (2016) Error sources in single-clinopyroxene thermobarometry and a mantle geotherm for the Novinka kimberlite, Yakutia. Am Mineral 101:2222–2232